

# Experimental Demonstration of In-Plane Negative-Angle Refraction with an Array of Silicon Nanoposts

Aimin Wu,<sup>†,§</sup> Hao Li,<sup>†</sup> Junjie Du,<sup>‡</sup> Xingjie Ni,<sup>§</sup> Ziliang Ye,<sup>§</sup> Yuan Wang,<sup>§</sup> Zhen Sheng,<sup>†</sup> Shichang Zou,<sup>†</sup> Fuwan Gan,<sup>\*,†</sup> Xiang Zhang,<sup>\*,§,||</sup> and Xi Wang<sup>\*,†</sup>

<sup>†</sup>State Key Laboratory of Functional Materials for Informatics, Shanghai Institute of Microsystem and Information Technology, Chinese Academy of Sciences, Shanghai 200050, China

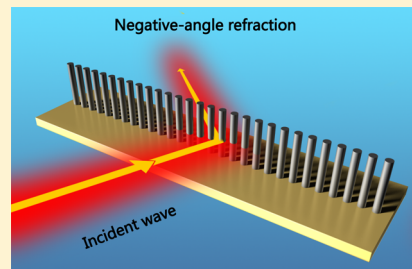
<sup>‡</sup>Quantum Institute for Light and Atoms, Department of Physics, East China Normal University, Shanghai 200062, China

<sup>§</sup>NSF Nanoscale Science and Engineering Center, University of California, 3112 Etcheverry Hall, Berkeley, California 94720, United States

<sup>||</sup>Department of Physics, King Abdulaziz University, Jeddah 21589, Saudi Arabia

## S Supporting Information

**ABSTRACT:** Controlling an optical beam is fundamental in optics. Recently, unique manipulation of optical wavefronts has been successfully demonstrated by metasurfaces. However, these artificially engineered nanostructures have thus far been limited to operate on light beams propagating out-of-plane. The in-plane operation is critical for on-chip photonic applications. Here, we demonstrate an anomalous negative-angle refraction of a light beam propagating along the plane, by designing a thin dielectric array of silicon nanoposts. The circularly polarized dipoles induced by the high-permittivity nanoposts at the scattering resonance significantly shape the wavefront of the light beam and bend it anomalously. The unique capability of a thin line of the nanoposts for manipulating in-plane wavefronts makes the device extremely compact. The low loss all-dielectric structure is compatible with complementary metal-oxide semiconductor technologies, offering an effective solution for in-plane beam steering and routing for on-chip photonics.



**KEYWORDS:** Negative-angle refraction, silicon nanoposts, circularly polarized dipoles, resonant particle, on-chip beam steering, nanophotonics

Arbitrary tailoring the light sources' properties brings a variety of new optical functions in optical communications, display technology, and optical data storage. For instance, the light sources with spatially varying polarizations find important applications in nanoscale high-resolution imaging and optical manipulation.<sup>1</sup> Optical beams endowed with large angular momentum have been successfully applied in optically driven micromachines,<sup>2</sup> micro/nano particles trapping,<sup>3</sup> and quantum information processing.<sup>4</sup> According to Huygens–Fresnel principle, peculiarly designed secondary sources consisting of resonant particles can lead to unconventional behaviors of the light in the far field, for example, negative-angle refraction,<sup>5–10</sup> total omnidirectional reflection,<sup>11</sup> electromagnetic (EM) superscattering,<sup>12</sup> and the guiding of EM waves.<sup>13,14</sup> In this Letter, we construct an upright interface consisting of a line of high-permittivity dielectric nanoposts that support circularly polarized dipoles (CPDs). These CPDs act as secondary sources in the interface with which on-chip optical beam steering can be achieved. Our theoretical calculations show that each silicon nanopost supports a CPD when it is on the resonance state while being kept at subwavelength scale. With an appropriate design, these nanoposts will thus have a unique scattering property. As a result, the wavefront of incident light can be significantly altered when it interacts with

the nanoposts array and the refracted beam will propagate in a negative angle, namely, the refracted beam lies on the same side of the normal as the incident beam. In addition to exceptional abilities of the CPDs on the near-field manipulation of surface plasmon as an unconventional wave source,<sup>15</sup> here we experimentally illustrate for the first time the remarkable capability of the CPDs in far-field beam manipulation.

Conventionally, bending of light beams in integrated optical circuits is realized by dielectric reflectors, photonic crystal devices, or metallic nanostructures.<sup>16–18</sup> Dielectric elements based on multilayer interference and the photonic band gap show low absorption loss but need a large thickness of at least several wavelengths. The metallic counterparts provide the subwavelength scale, but typically suffer from intrinsic absorption loss. The recent realization of metasurfaces consisting of arrangement of nanoantennas offers tremendous freedom in manipulating optical wavefronts.<sup>19–28</sup> However, these specially engineered metasurfaces have thus far been limited to operate on light beams propagating out-of-plane.

**Received:** December 24, 2014

**Revised:** February 5, 2015

**Published:** February 9, 2015

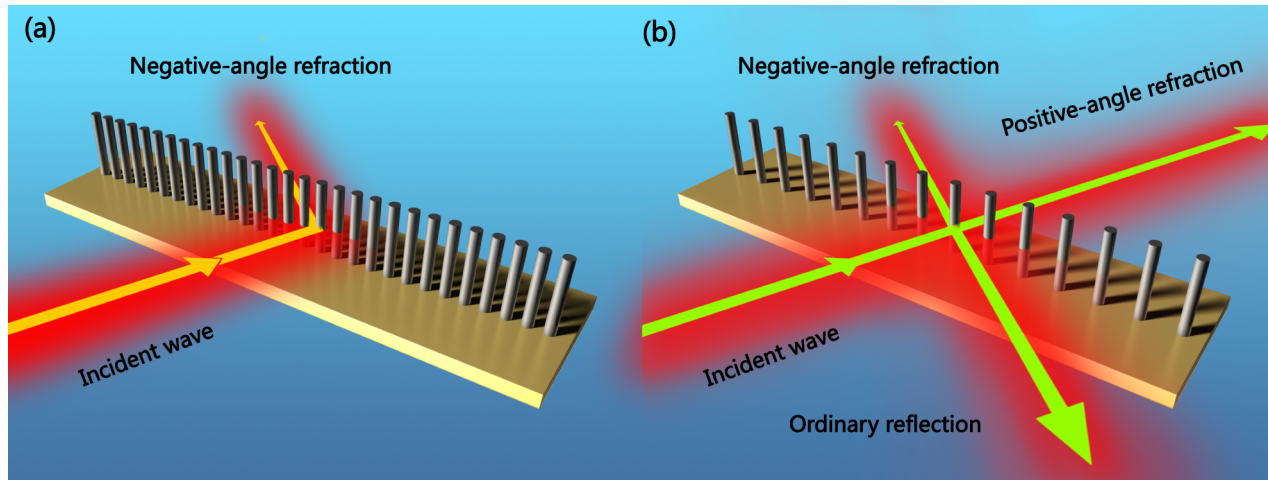


**Figure 1.** Schematic of light beam propagation through an upright nanoposts interface. (a) Negative-angle refraction through the upright interface consisting an array of Si nanoposts. (b) All the possible diffraction orders for conventional nanoposts array, supporting the 0th and  $-1$ st refracted and reflected orders. The negative-angle refraction, positive-angle refraction, and ordinary reflection are corresponding to  $-1$ st order refraction, 0th order refraction, and 0th order reflection, respectively.

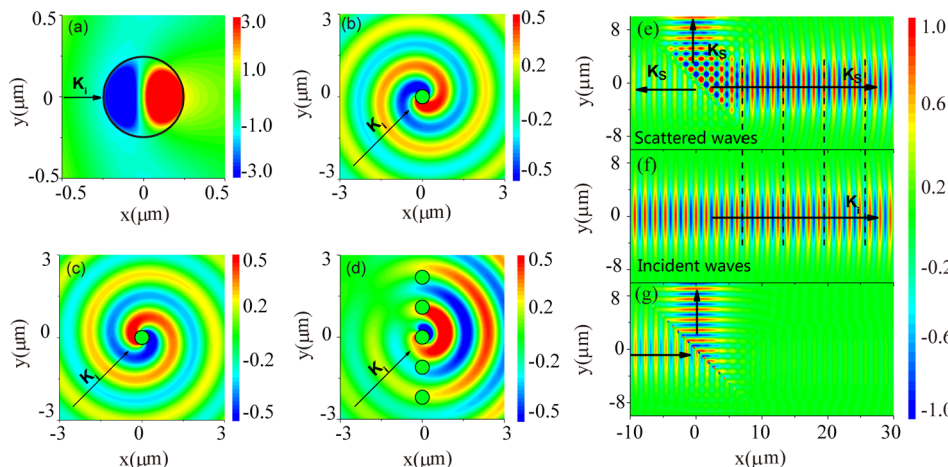


**Figure 2.** CPDs in the upright nanopost interface for the negative-angle refraction. (a) The  $H$  field distribution at the resonance of the 1st AMC when a light beam illuminating a single isolated nanopost, showing a dipole-shape. The scattered  $H$  field of the  $n = -1$  (b) and  $n = +1$  (c) component, each of which denotes a CPD with the same amplitude but opposite rotating momentum for a single isolated nanopost case, thus the summation creates the linearly oscillating dipole. (d) The scattering of a nanopost in the array, which is the summation of  $n = +1$  and  $n = -1$  CPD components and  $n = 0$  isotropic component,  $b_{-1}$  is three times as large as  $b_{+1}$  component, and  $b_0$  is even smaller as the resonance is in the 1st AMC. Each nanopost in the array scatters no light to the ordinary reflection direction at this particular resonant state. The scattered field (e) and the corresponding incident field (f) of the nanoposts array. (g) The total field. The cancellation of the scattered field and the incident field in the positive angle indicates the elimination of the positive-angle refraction.  $\mathbf{K}_s$  and  $\mathbf{K}_i$  denotes the wave vector of the scattered and incident wave.

Therefore, it is extremely appealing to exploit an interface composed of a single layer of silicon nanoposts as a new beam control approach for on-chip photonic applications when considering system miniaturization and integration. First of all, silicon nanoposts can be easily integrated, as they are fabricated upright on the substrate, and the light propagation is parallel to the substrate, which is necessary for the integration with other planar optical components. Second, silicon nanoposts have negligible absorption loss in contrast to the metallic structures at the optical communication wavelength range. The total negative-angle transmission efficiency can reach over 90% through rigorous design, which makes the single layer array practically promising for integrated optical circuits. Last but not least, the complementary metal-oxide semiconductor (CMOS) compatibility of the thin line of silicon nanoposts

makes it a perfect new component for electro-optical integration trend in silicon photonics.

The negative-angle refraction we demonstrate is realized in a single line of upright silicon nanoposts shown in Figure 1a. This artificially engineered interface, when considered as a first-order grating, can simultaneously support the 0th and  $-1$ st order refraction and reflection. All the permitted directions of the outgoing beam are schematically indicated in Figure 1b. However, a counterintuitive phenomenon occurs in our structure, where the ordinary reflection and refraction are completely suppressed. Most of the energy in the beam propagates in the negative refracted angle, as shown in Figure 1a. Our studies show that this effect is attributed to the excitation and tailoring of the CPDs inside the high permittivity nanoposts at the dipole resonant condition when it is properly arranged in

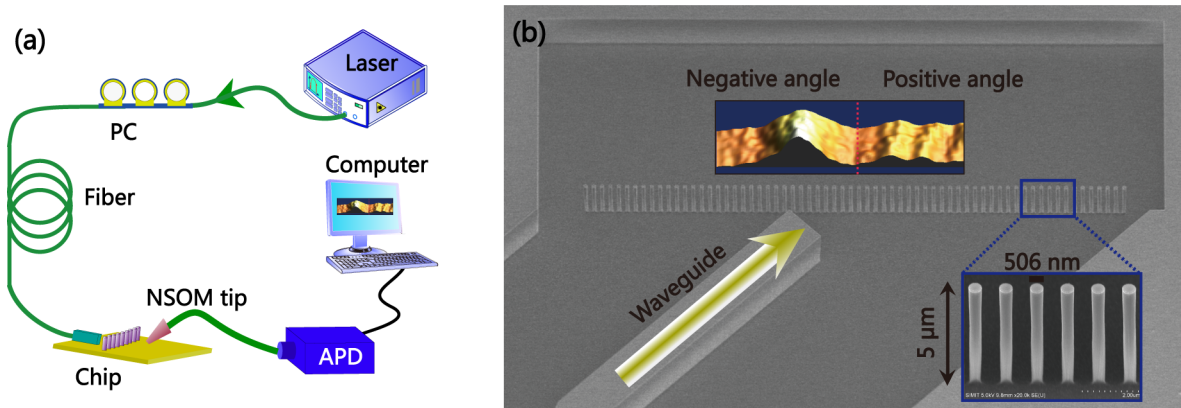


**Figure 3.** Negative-angle refraction demonstration with NSOM. (a) The experimental layout for the NSOM measurement. The nanoposts array is illuminated by a laser beam at a  $45^\circ$  incident angle through a silicon optical waveguide. The desired polarization ( $H$  field polarized along the nanopost) is attained by a polarization controller. The field distribution is obtained using a NSOM probe. (b) The SEM image of the entire structure includes the waveguide and the nanoposts array. The bottom inset shows the fabricated silicon nanoposts that have a height of  $5\ \mu\text{m}$  and a diameter of  $506\ \text{nm}$ . The top inset shows the scanned 3D-NSOM image in which the remarkable difference of the transmission in the negative angle and the positive angle is demonstrated. The red dotted line indicates the normal.

an array. Considering the 2D case where the field is uniform in the  $z$ -direction and the magnetic ( $H$ ) field is polarized along  $z$ , the scattering  $H$  field of a silicon nanopost can be expressed as in the Mie expansion form<sup>29</sup>

$$H_{\text{sca}} = \sum_{n=-\infty}^{+\infty} i^n b_n H_n^{(1)}(k_b r) e^{in\phi} \quad (1)$$

Here  $r$  and  $\phi$  are the polar coordinates,  $H_n$  is the Hankel function of the first kind,  $b_n$  is the Mie scattering coefficient, and  $k_b$  is the wave number in the background medium.

As shown in Figure 2a, the  $H$  field pattern exhibits the dipole symmetry at resonance in the first angular momentum channel (AMC) corresponding to the incident wavelength of  $1550\ \text{nm}$  for an isolated single nanopost with radius  $r_s = 255\ \text{nm}$ . According to eq 1, this dipolar symmetry is from the summation of the two components  $n = +1$  and  $n = -1$  that denote a clockwise and counterclockwise CPD moment, respectively, as shown in Figure 2b,c. As the two components have the same amplitude and a definite phase difference, the superposition will result in a linearly oscillating dipole. When the silicon nanoposts are arrayed in the line, the induced high magnitude charges in the nanoposts strengthen the interaction. Therefore, unlike the single isolated case that the components  $n = +1$  and  $n = -1$  behave as a whole, the optical behavior of angular momenta components of opposite signs is not symmetrical and can be independently manipulated. Either of the two components can be tailored to be much larger than the other by changing the nanopost separation and the incident angle, implying that only one CPD becomes dominant. The superposition of the CPDs and the  $n = 0$  component (very small at the resonance in the first AMC) will thus provide the possibility to achieve the exceptional radiation property under specific design. The importance of the CPD is also manifested by the comparison of the remarkable different field distribution of the nanoposts array at resonance in different AMCs in ref 5.

In our structure, the period is set as  $\lambda/\sqrt{2}$ . The calculation shows that at  $45^\circ$  incidence, the amplitude of the  $n = -1$  component is about as three times large as that of the  $n = +1$  component. The superposition of these specific CPDs and the  $n = 0$  component will make each nanopost a unique secondary source, which also shows quasi-CPD symmetry. These unique

secondary sources in the array radiate in a strikingly different way, that is, it scatters no light in the ordinary reflected direction as shown in Figure 2d,e. While the scattered field in the positive refracted angle cancels out the incident field, thus only the negative-angle outgoing beam is left in the transmitted field. Supporting Information Movies 1 and 2 demonstrate the anomalous negative-angle refraction phenomenon and exciting of the quasi-CPD in each silicon nanopost. According to theoretical simulation, this upright dielectric interface can redirect the incident beam with 93% efficiency into the bending beam by spatially tailoring the geometry of the resonators and hence their scattering property in the array.<sup>5</sup>

This phenomenon is directly verified by a near-field scanning optical microscope (NSOM) as shown in Figure 3a. A silicon waveguide directs the optical beam with the  $H$ -polarization along the nanopost toward the line at  $45^\circ$ , and the NSOM probe recorded the field intensity at the transmission side. Scanning electron microscope (SEM) images of the fabricated structure are shown in Figure 3b. The interface consists of a single line of  $5\ \mu\text{m}$  high silicon nanoposts standing on top of a silicon oxide layer. The radius of the post and the period are  $r_s = 253\ \text{nm}$  and  $a_0 = \lambda/\sqrt{2}$ , respectively, where  $\lambda = 1550\ \text{nm}$  is the wavelength of the incident beam. The top inset in Figure 3b shows that the measured field intensity in the negative angle is remarkably larger than that in the positive angle, demonstrating the negative-angle refraction of the beam. Nevertheless, the near-field mean cannot provide the propagating information on the outgoing beam due to the limited scanning range of the NSOM. Hence, we characterize the device's far-field response in the following section.

For the far-field measurement, the incident beam illuminates the line of the nanoposts in a similar configuration on the chip. An overhead infrared camera (Hamamatsu C2741) is used to measure the propagation path of the wave by imaging the scattering spot produced when the beam encounters nanoposts, the sidewall of the etched trench, and the scanning fiber. The position of the fiber is indicated by the yellow dashed line. As shown in both Figure 4a,b, the strong scattering can be seen when the light illuminates at the interface. The fiber produces the scattered spot only when it is located at the same side of the normal as the incident light beam. The remarkable contrast of the scattering on the fiber at different positions provides

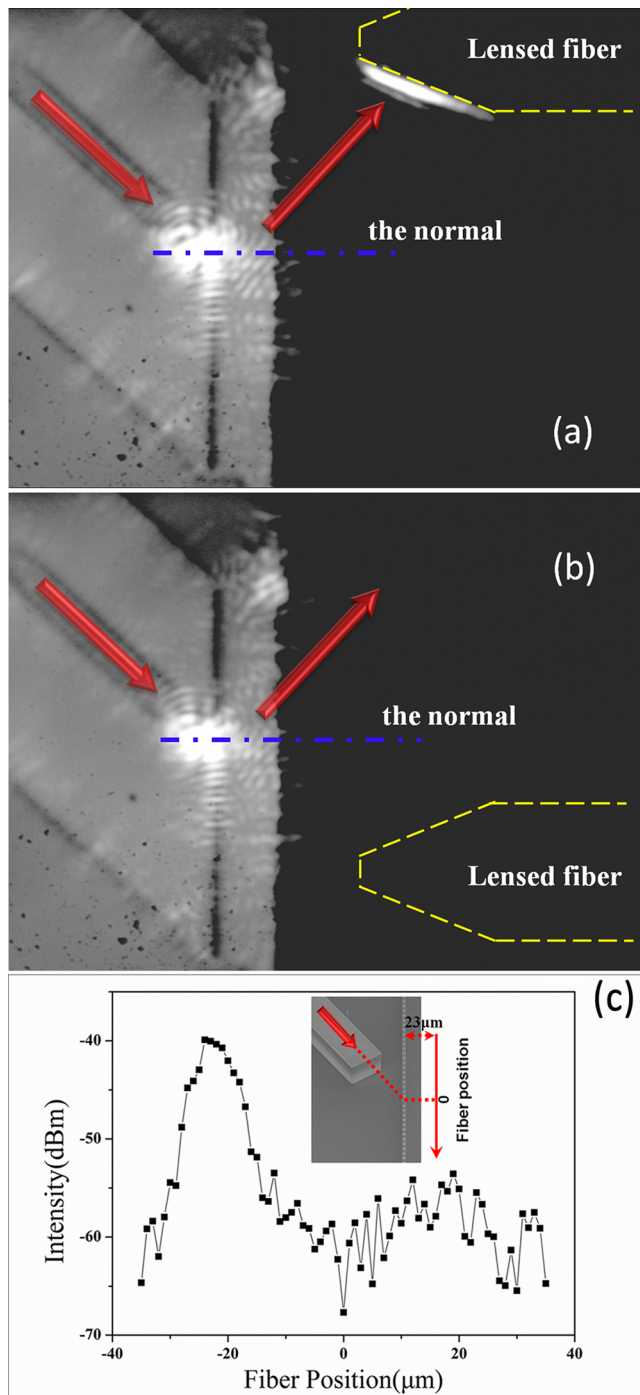


**Figure 4.** Far-field measurements. Images taken by the top IR camera when the optical fiber located at different sides of the normal plane: (a) negative angle side and (b) positive angle side. The strong scattering of the negative transmitted beam with the fiber can be clearly observed, while no scattering can be seen in the positive direction. (c) Transmission power versus the fiber scanning position. The inset illustrates the moving path of the fiber in the experiment. The peak value in the negative angle side is 13 dB larger than that of the positive angle side. The crossing point of the extension line from the waveguide and the nanoposts array is set as  $x = 0$ . The distance between the fiber and the nanoposts line is  $23 \mu\text{m}$ , and the peak transmission position is detected at  $x = -23 \mu\text{m}$ , indicating a  $90^\circ$  sharp turn of the beam. The red arrows in (a) and (b) show the incident beam in the waveguide and the refracted beam from the nanoposts array. The yellow dashed lines indicate the fiber.

another evidence of the negative-angle refraction. Meanwhile, no scattering is observed in the ordinary reflection direction, indicating the complete suppression of this reflection, which agrees well with the theoretical results because those particular secondary sources do not radiate light in this direction.

The fiber in the setup is also used to record the optical power at different positions of the transmission side. Details of far-field measurement can be found in Methods (Supporting Information). As shown in Figure 4c, a sharp peak is detected in the negative angle side, and a much lower peak appears in the positive angle side. The difference of the optical intensity between the two peaks is more than 13 dB, which means over 96% of the refracted wave propagates in the negative angle. The existence of the very weak optical wave in the positive angle is partially caused by the nonuniformity of the radius of nanoposts from top to bottom. According to the geometry analysis in Figure 4c, we conclude that the beam makes a substantial  $90^\circ$  sharp bending through the negative-angle refraction.

A wide incident angle of the interface is another critical parameter for on-chip optical network and interconnection, providing flexibility for chip design. The beam bending through the interface can be achieved over a wide angle range, varying from  $35^\circ$  to  $60^\circ$ . To this end, the nanoposts array is fabricated in a large rectangle trench and its SEM image is given in Figure 5a. The scattering spots on the interface and the sidewall of the trench imaged by the overhead infrared camera is used to show the propagation properties of the beam. The incoming beam is guided by lensed fiber to illuminate the line directly in order to conveniently change the incident angle. In Figure 5b-d, the beams have the angle of incidence to be  $35^\circ$ ,  $45^\circ$ , and  $60^\circ$ , respectively. It is shown that in all the cases the beams make a sharp bend close to  $90^\circ$  to the negative angle and negligible ordinary reflection is observed, indicating this unconventional optical behavior occurs in the wide angle range of  $35^\circ$  to  $60^\circ$ . Note that very weak scattering in the positive angle is observed at the trench sidewall in Figure 5b-d, partially due to the fabrication imperfection. While at the incidence angle of  $35^\circ$  and  $60^\circ$ , the weak scattering in the positive angle is slightly increased compared with  $45^\circ$ , which is consistent with the theoretical prediction in Supporting Information Figure S3.

As a comparison, we also demonstrate the far-field propagation property of a control sample in Supporting Information Figure S4, where the line is comprised of silicon nanoposts at the resonance in the 0th AMC. Therefore, the  $n = 0$  component with the isotropic symmetry will dominate in this case. The same period configuration is utilized to support the  $-1\text{st}$  and 0th order diffraction. The four outgoing beams with comparable intensity corresponding to the  $-1\text{st}$  and 0th order diffraction direction is observed, indicating that the anomalous negative-angle refraction only occurs when the dominant CPDs are excited in the interface.

In summary, we experimentally demonstrate negative-angle beam bending based on a single line of 5- $\mu\text{m}$ -high upright silicon nanoposts. The underneath physics is that the excited CPDs in the nanoposts form a particular secondary source in the line that alters the outgoing wavefronts. This anomalous phenomenon paves a new way for on-chip beam control such as steering, routing, and filtering for optical communications.

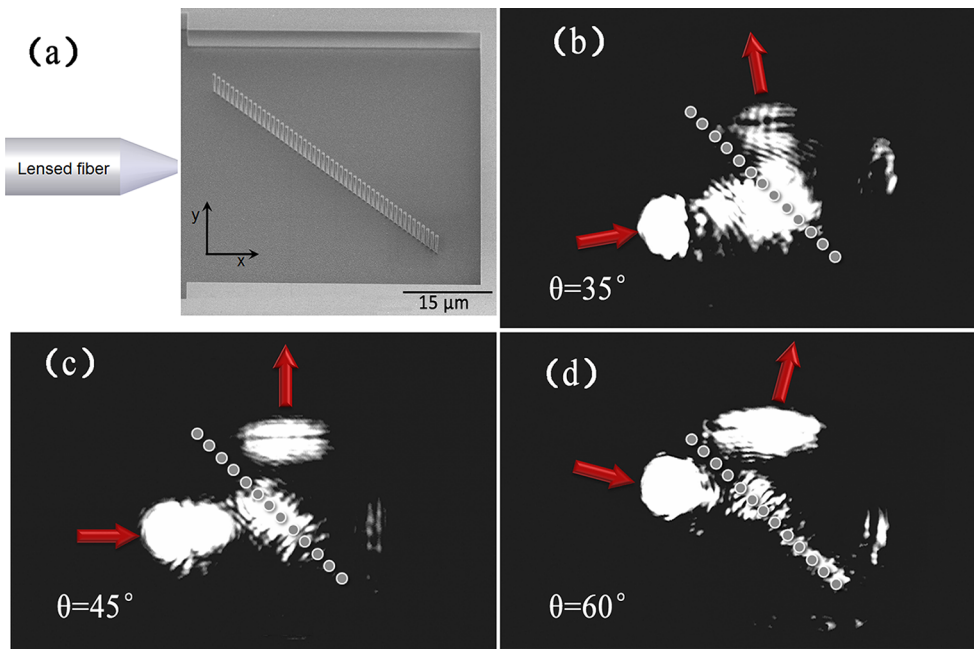


**Figure 5.** Experimental demonstration of wide incident angle of the beam bending. (a) Tilted SEM image of the nanoposts array. The fiber is artificially added to show that the incoming beam is directly guided by lensed fiber to the interface. (b–d) Top view of the beam propagation by the top infrared camera with an incident angle of 35°, 45°, and 60° that are reached by rotation of the sample. The light beams make sharp bending around 90° in all the cases, consistent with the prediction by the grating equations for the array. The scattering spots in the positive angle in 35° and 60° are slightly increased comparing with 45° case, indicating the limitation of the incident angle range. The red arrows schematically show the direction of the incident beam and the negative-angle refracted beam. The circles illustrate the position of the nanoposts.

## ■ ASSOCIATED CONTENT

### Supporting Information

Methods, supporting Movies 1 and 2, and Figure S1–S4. This material is available free of charge via the Internet at <http://pubs.acs.org>.

## ■ AUTHOR INFORMATION

### Corresponding Authors

\*E-mail: (F.G.) [fawan@mail.sim.ac.cn](mailto:fawan@mail.sim.ac.cn).

\*E-mail: (X.Z.) [xiang@berkeley.edu](mailto:xiang@berkeley.edu).

\*E-mail: (X.W.) [xwang@mail.sim.ac.cn](mailto:xwang@mail.sim.ac.cn).

### Author Contributions

A.W., H.L., and J.D. contributed equally to this work.

### Notes

The authors declare no competing financial interest.

## ■ ACKNOWLEDGMENTS

This work was partially supported by Natural Science Foundation of China (Grants 61107031, 61275112, 11474098, and 61401443), Natural Science Foundation of Shanghai (Grant 11ZR1443700). J.D. is supported by Innovation Program of Shanghai Municipal Education Commission (Grant 4ZZ049). This work was also partially supported by U.S. Air Force Office of Scientific Research (AFOSR) MURI program (Grant FA9550-12-1-0024). We thank M. H. Qi for helpful discussions.

## ■ REFERENCES

- (1) Zhan, Q. *Adv. Opt. Photonics* **2009**, *1*, 1–57.
- (2) Knöner, G.; Nieminen, T.; Loke, V.; Heckenberg, N.; Rubinsztein-Dunlop, H. *Opt. Express* **2007**, *15*, 5521–5530.
- (3) Ng, J.; Lin, Z. F.; Chan, C. T. *Phys. Rev. Lett.* **2010**, *104*, 103601.
- (4) Vaziri, A.; Pan, J.-W.; Jennewein, Th.; Weihs, G.; Zeilinger, A. *Phys. Rev. Lett.* **2003**, *91*, 227902.
- (5) Du, J. J.; Lin, Z. F.; Chui, S. T.; Lu, W. L.; Li, H.; Wu, A. M.; Sheng, Z.; Zi, J.; Wang, X.; Zou, S. C.; Gan, F. W. *Phys. Rev. Lett.* **2011**, *106*, 203903.
- (6) Peng, L.; Ran, L.; Chen, H.; Zhang, H.; Kong, J.; Grzegorczyk, T. *Phys. Rev. Lett.* **2007**, *98*, 157403.
- (7) Schuller, J.; Zia, R.; Taubner, T.; Brongersma, M. *Phys. Rev. Lett.* **2007**, *99*, 107401.
- (8) Liu, S.; Chen, W.; Du, J.; Lin, Z.; Chui, S.; Chan, C. *Phys. Rev. Lett.* **2008**, *101*, 157407.
- (9) Vynck, K.; Felbacq, D.; Centeno, E.; Căbuş, A.; Cassagne, D.; Guizal, B. *Phys. Rev. Lett.* **2009**, *102*, 133901.
- (10) Shelby, R. A.; Smith, D. R.; Schultz, S. *Science* **2001**, *292*, 77–79.
- (11) Du, J. J.; Lin, Z. F.; Chui, S. T.; Dong, G. J.; Zhang, W. P. *Phys. Rev. Lett.* **2013**, *110*, 163902.
- (12) Ruan, Z.; Fan, S. *Phys. Rev. Lett.* **2010**, *105*, 013901.
- (13) Maier, S. A.; Kik, P. G.; Atwater, H. A.; Meltzer, S.; Harel, E.; Koel, B. E.; Requicha, A. *Nat. Mater.* **2003**, *2*, 229–232.
- (14) Du, J.; Liu, S.; Lin, Z.; Zi, J.; Chui, S. *Phys. Rev. A* **2009**, *79*, 051801.
- (15) Rodríguez-Fortuño, F. J.; Marino, G.; Ginzburg, P.; O'Connor, D.; Martínez, A.; Wurtz, G. A.; Zayats, A. V. *Science* **2013**, *340*, 328–330.
- (16) John, S. *Phys. Rev. Lett.* **1987**, *58*, 2486–2489.
- (17) Yablonovitch, E. *Phys. Rev. Lett.* **1987**, *58*, 2059–2062.
- (18) Fink, Y.; Winn, J. N.; Chen, C.; Michel, J.; Joannopoulos, J. D.; Thomas, E. L. *Science* **1998**, *282*, 1679–1682.
- (19) Yu, N.; Genevet, P.; Kats, M. A.; Aieta, F.; Tetienne, J.; Capasso, F.; Gaburro, Z. P. *Science* **2011**, *334*, 333–337.
- (20) Ni, X. J.; Emani, N. K.; Kildishev, A. V.; Boltasseva, A.; Shalaev, V. *Science* **2011**, *335*, 427.
- (21) Aieta, F.; Genevet, P.; Yu, N.; Kats, M. A.; Gaburro, Z.; Capasso, F. *Nano Lett.* **2012**, *12*, 1702–1706.
- (22) Huang, L. L.; Chen, X. Z.; Muhlenbernd, H.; Li, G.; Bai, B. F.; Tan, Q. F.; Jin, G. F.; Zentgraf, T.; Zhang, S. *Nano Lett.* **2012**, *12*, 5750–5755.

- (23) Sun, S. L.; Yang, K. Y.; Wang, C. M.; Juan, T. K.; Chen, W. T.; Liao, C. Y.; He, Q.; Xiao, S. Y.; Kung, W. T.; Guo, G. Y.; Zhou, L.; Tsai, D. P. *Nano Lett.* **2012**, *12*, 6223–6229.
- (24) Pfeiffer, C.; Grbic, A. *Phys. Rev. Lett.* **2013**, *110*, 197401.
- (25) Kildishev, A. V.; Boltasseva, A.; Shalaev, V. M. *Science* **2013**, *339*, 1232009.
- (26) Yu, N. F.; Capasso, F. *Nat. Mater.* **2014**, *13*, 139–150.
- (27) Lin, D. M.; Fan, P. Y.; Hasman, E.; Brongersma, M. L. *Science* **2014**, *345*, 298–302.
- (28) Pfeiffer, C.; Emani, N. K.; Shaltout, A. M.; Boltasseva, A.; Shalaev, V. M.; Grbic, A. *Nano Lett.* **2014**, *14*, 2491–2497.
- (29) Van de Hulst, H. C. *Light Scattering by Small Particles*; Dover: New York, 1981.